Finger capacitance of a terahertz photomixer in low-temperature-grown GaAs using the finite element method*

Chen Long-Chao(陈龙超) and Fan Wen-Hui(范文慧)†

State Key Laboratory of Transient Optics and Photonics, Xi'an Institute of Optics and Precision Mechanics, Chinese Academy of Sciences, Xi'an 710119, *China*

(Received 15 January 2012; revised manuscript received 12 March 2012)

Interdigitated finger capacitance of a continuous-wave terahertz photomixer is calculated using the finite element method. For the frequently used electrode width (0.2 μm) and gap width (1.8 μm), the finger capacitance increases quasi-quadratically with the number of electrodes increasing. The quasi-quadratic dependence can be explained by a sequence of lumped capacitors connected in parallel. For a photomixer composed of 10 electrodes and 9 photoconductive gaps, the finger capacitance increases as the gap width increases at a small electrode width, and follows the reverse trend at a large electrode width. For a constant electrode width, the finger capacitance first decreases and then slightly increases as the gap broadens until the smallest finger capacitance is formed. We also investigate the finger capacitances at different electrode and gap configurations with the 8 μm × 8 μm photomixer commonly used in previous studies. These calculations lead to a better understanding of the finger capacitance affected by the finger parameters, and should lead to terahertz photomixer optimization.

Keywords: terahertz photomixer, continuous-wave, interditated finger capacitance, finite element method

PACS: 41.20.Cv, 02.70.Dh, 42.72.Ai **DOI:** 10.1088/1674-1056/21/10/104101

1. Introduction

By using an interdigitated metal finger coupled to a planar photoconductive (PC) antenna fabricated in low-temperature-grown GaAs (LTG-GaAs), the terahertz (THz) optical-heterodyne conversion or photomixing technique initiated by Brown *et al.*,[1] has been spread and developed. In a photomixer, two above-bandgap continuous-wave (CW) visible or near-infrared frequencies are combined, generating a beat optical signal at the THz frequency, which modulates the conductivity of a PC switch in the interdigitated finger region via photogenerated electron–hole pairs. In the presence of an external bias voltage applied to the photomixer, the resulting THz current drives the PC antenna and generates CW monochromatic THz radiation in free space. Since these all-PC systems can be driven by inexpensive, compact and tunable diode lasers,[2,3] they may become compact, low-power consuming, and cost-effective commercial terahertz products.[4] The narrow spectral bandwidth and tunable frequency of the photomixers make them attractive sources for local-oscillator heterodyne detection in astronomy,[5] high-resolution molecular spectroscopy,[6,7] and medical imaging.[8]

However, low output power is the most intractable issue that has impeded efficient use of THz photomixers in some applications, such as local oscillators in communications and heterodyne detection systems. As shown in Fig. 1(a), a photomixer is composed of an interdigitated metal finger connected to a bow-tie antenna with a bias voltage $V_{\rm B}$. All of the metal structure is fabricated on the surface of LTG-GaAs. Figure 1(b) is the equivalent circuit diagram for the photomixer, where $R(t)$ is the modulated resistance of the PC gap. According to this equivalent circuit, the output spectra of a photomixer can be expressed by a two-time-constant expression as[9]

$$P(\omega) = \frac{P_0}{[1+(\omega\tau_{\rm eh})^2][1+(\omega R_{\rm A}C)^2]}, \qquad (1)$$

where ω is the frequency of THz wave, P_0 is the reference output power at low frequencies, $\tau_{\rm eh}$ is the pho-

*Project supported by the National High Technology Research and Development Program of China (Grant No. 2011AAxxx2008A), Hundred Talent Program of the Chinese Academy of Sciences (Grant No. J08-029), and the Main Direction Program of Knowledge Innovation of the Chinese Academy of Sciences (Grant No. YYYJ-1123-4).

†Corresponding author. E-mail: fanwh@opt.ac.cn

© 2012 Chinese Physical Society and IOP Publishing Ltd

tocarrier lifetime, R_A is the radiation impendence of planar PC antenna, and C is the interdigitated finger capacitance. It shows that on the higher-frequency side, the output power is influenced by τ_{eh} and $R_A C$ and decreases dramatically by 12 dB/octave. Therefore, in order to produce high output power, both photocarrier lifetime τ_{eh} and interdigitated finger capacitance C should be optimized to be as small as possible. Photocarrier lifetime τ_{eh} is determined by LTG-GaAs that has been optimized previously,[10,11] and capacitance C is determined by the geometric structure of an interdigitated metal finger that has never been optimized.

In this paper, by using the finite element method (FEM), we calculate the interdigitated finger capacitances of a CW-THz photomixer in different device configurations in order to optimize the photomixer design. According to the simulated results, it is found that the values of finger capacitance have been obviously influenced by the number of metal fingers N_e, electrode width L_e, and PC gap width L_g. The dependence between finger capacitance and different photomixer configurations reveals a very useful way to optimize THz photomixers.

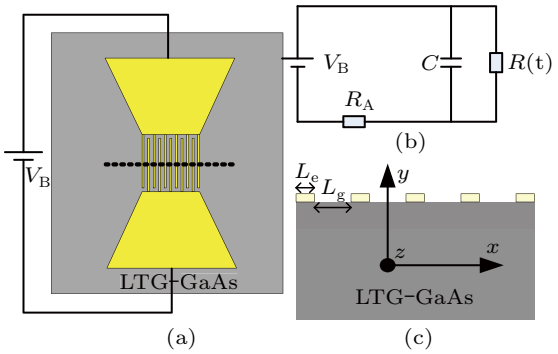


Fig. 1. (colour online) (a) Top view of the interdigitated finger structure commonly used in a CW-THz photomixer, consisting of a bow-tie PC antenna coupled to the external circuit, (b) equivalent circuit diagram for the photomixer and antenna, and (c) cross-sectional view of active region along dashed line shown in panel (a).

2. FEM analysis for finger capacitance

The finite element method (FEM) is the most effective method to use in complicated geometries.[12] Based on this method, we attained the finger capacitance when the parameters of interdigitated finger, such as electrode number N_e, electrode width L_e, and gap width L_g, are changed freely. For simplicity, we make the following assumptions concerning the interdigitated finger photomixer. (i) A static bias voltage V_B applied to two adjacent electrodes can be used in this simulation. In practical work, the bias V_B was alternated to facilitate lock-in detection, but the dielectric relaxation time is far less than the period of the alternated bias so that the dielectric polarization of the device, hence the capacitance, is unaffected. (ii) No free charges exist in the PC gap. It can be explained as follows: first, before the beat laser drives the photomixer, no photocarrier electron–hole pairs are generated in the PC gap. Second, LTG-GaAs can be treated as insulator that has an estimated bulk resistivity of $\sim 10^7$ Ω·m so that the electrical current driven by V_B is very small. (iii) All of the metal electrodes are in the state of electrostatic equilibrium. This is because metal electrodes are perfect electrical conductors composed of Cr and Au. Based on this assumption, metal electrodes can be viewed as equalpotential object in order to the simplify boundary condition. (iv) Considering that the spot of the beat laser is circular, the active area is assumed to be a square in order to use the active area sufficiently. Based on assumption (ii) and electrostatic theory, the scalar electric potential $\Phi(x, y, z)$ of the interdigitated finger area of the photomixer obeys Laplace's equation and can be expressed as

$$\nabla \cdot \nabla[\Phi(x, y, z)] = \nabla^2 \Phi(x, y, z) = 0. \qquad (2)$$

Figure 1(c) is the cross-sectional view of active region along the dashed line shown in Fig. 1(a). The coordinate system is shown in Fig. 1(c). Considering the symmetrical characteristic in the central xoy plane and periodical characteristic along the x axis, we only need to simulate an elementary unit of the photomixer. The length of the unit along x axis is $2L$ ($-L \sim +L$), and the thickness of the unit along y axis is $2D$ ($-D \sim +D$) as shown in Fig. 2. The electrical field E in the central yoz plane between two adjacent electrodes is perpendicular to this plane, so the potential gradient in this plane along the x axis is zero. The two metal electrodes are biased by an external field, so the boundary condition of the interface between the electrode and LTG-GaAs is of a Dirichlet boundary. The electric potential of the electrode in the left of the y axis is $\Phi = V_B/2$, and the right one is $\Phi = -V_B/2$. The zero potential plane is the undersurface of photomixer. Definitions of boundary conditions are shown in Table 1.

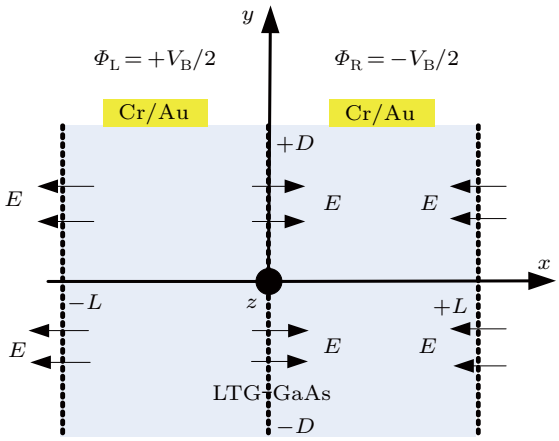


Fig. 2. (colour online) Schematic diagram of the boundary condition in the central cross-section of an elementary unit in a photomixer along the *xoy* plane.

Table 1. Definitions of boundary conditions, $\boldsymbol{n}$ represents the normal vector of *yoz* plane.

$x = -(L_e + L_g/2) \sim -L_g/2,\ y = D$	$\Phi = V_B/2$
$x = -L \sim L,\ y = -D$	$\Phi = 0$
$x = -L,\ y = 0$	$\partial\Phi/\partial\boldsymbol{n} = 0$

A tetrahedral mesh is utilized in this simulation. The FEM calculations provide the nodal potential of the tetrahedral mesh for calculating potential distributions in other parts of the tetrahedral mesh, which satisfies the following linear matrix equation:

$$\boldsymbol{K\Phi} = 0, \tag{3}$$

where $\boldsymbol{K}$ is the coefficient matrix and Φ is the potential matrix of nodal potential. Thus, the discrete form of Eq. (3) is

$$\sum_{j=1}^{n} K_{ij}\varphi_j = 0, \quad (i = 1, 2, \ldots, n), \tag{4}$$

where ϕ_j is the nodal potential of all vertices of tetrahedral mesh; n is the total number of tetrahedral meshes, and it is sensitive to both the accuracy and duration of the calculation. Here, we choose the edge length of a tetrahedral mesh that is one percent of the whole active area in size. According to Eq. (2) and variational method, the matrix element of $\boldsymbol{K}$ is obtained as

$$\begin{aligned} K_{ij} &= \int_{\Omega} \nabla\Psi_i \cdot \nabla\Psi_j \,\mathrm{d}\Omega \\ &= \sum_{e=1}^{e_n} \int_{\Omega^e} \nabla\Psi_i^e \cdot \nabla\Psi_j^e \,\mathrm{d}\Omega = \sum_{e=1}^{e_n} K_{ij}^e, \end{aligned} \tag{5}$$

where Ω represents the whole volume of the photomixer, Ω^e is the volume of the elementary tetrahedral mesh, e_n is the marker sign of each tetrahedral mesh, Ψ_i^e is cardinal interpolation function related to the tetrahedral mesh and has the following form:

$$\Psi_i^e = \sum_{i=1}^{4} (p_i + q_i x + r_i y + s_i z), \tag{6}$$

where p_i, q_i, r_i, and s_i are interpolation coefficients determined by the position of tetrahedral mesh. $i = 1$, 2, 3, 4 represent the four vertices of tetrahedral mesh. According to Eqs. (5) and (6), matrix equation (4) can be calculated numerically. The normalized potential distribution of an elementary unit in the photomixer is shown in Fig. 3.

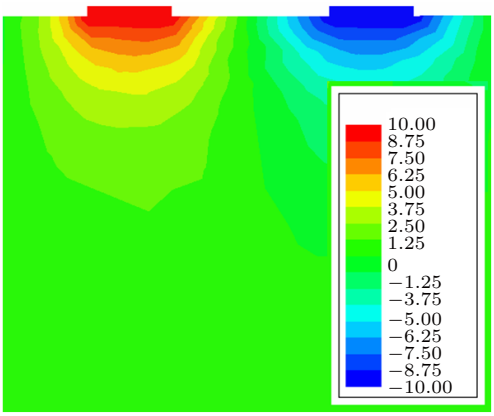


Fig. 3. (colour online) Normalized electric potential distribution in the central cross-section of the photomixer along the *xoy* plane.

Other field quantities, such as electrical field $E(x, y, z)$ and electrical displacement field $D(x, y, z)$, can be obtained from Maxwell's differential equations as

$$\begin{aligned} E(x, y, z) &= -\nabla\Phi(x, y, z), \\ D(x, y, z) &= -\varepsilon_r\varepsilon_0\nabla\Phi(x, y, z), \end{aligned} \tag{7}$$

where ε_r is 12.8 for GaAs, and ε_0 is the permittivity of free space. According to electrostatic energy storage theory, electrostatic energy stored in interdigitated photomixer has the following form

$$\begin{aligned} W &= \frac{1}{2}\int_{\Omega} D \cdot E \,\mathrm{d}\Omega = \frac{1}{2}\int_{\Omega} \varepsilon_0\varepsilon_r \left|\nabla\Phi(x, y, z)\right|^2 \mathrm{d}\Omega \\ &= \frac{1}{2}\varepsilon_0\varepsilon_r \sum_{e=1}^{e_n} \int_{\Omega^e} \left[\left(\frac{\partial\Phi}{\partial x}\right)^2 + \left(\frac{\partial\Phi}{\partial y}\right)^2 \right. \\ &\quad \left. + \left(\frac{\partial\Phi}{\partial z}\right)^2\right] \mathrm{d}\Omega^e. \end{aligned} \tag{8}$$

Finally, finger capacitance can be calculated from the following formula

$$\begin{aligned} C &= \frac{2W}{V_B} \\ &= \frac{\varepsilon_0\varepsilon_r}{V_B} \sum_{e=1}^{e_n} \int_{\Omega^e} \left[\left(\frac{\partial\Phi}{\partial x}\right)^2 + \left(\frac{\partial\Phi}{\partial y}\right)^2 + \left(\frac{\partial\Phi}{\partial z}\right)^2\right] \mathrm{d}\Omega^e. \end{aligned} \tag{9}$$

In this calculation, we assume electrode width L_e and gap width L_g to vary from 0.1 μm to 10.0 μm and the number of electrode, N_e, to change from 2 to 10. The active area of photomixer is expressed as $S = [N_e L_e + (N_e - 1)L_g]^2$, that is to say, the active area of the interdigitated finger calculated varies from 0.09 μm^2 to 8.41 × 10^4 μm^2.

3. Results and discussion

One important issue in designing photomixers is the dependence of capacitance and electrode number for the given electrode width and gap width. In previous work,[13] it was found that the change in the trap occupation of the photoconductor close to metal–semiconductor junction will give a highly non-uniform electric field distribution, leading to some phenomena such as near-anode enhancement. Since the bias is alternated with respect to facilitate lock-in detection, this phenomenon can be seen near both electrodes. In order to make these two enhanced fields overlap in the PC gap, the optimum electrode width and gap width are fabricated to be 0.2 μm and 1.8 μm, respectively. The capacitance is plotted in Fig. 4 as a function of the electrode number for the photomixer with a fixed gap width (1.8 μm) and electrode width (0.2 μm). In this case, the electrode number increases from 2 to 10, and its corresponding active area varies from 4.84 μm^2 to 331.2 μm^2, which generates a minimum and maximum capacitance of 0.07 fF and 4.84 fF, respectively. If the photomixer is fitted with a broadband spiral antenna, whose radiation resistance is given by

$$R_A = \frac{60\pi}{[(\varepsilon_r + 1)/2]^{1/4}} = 70\ \Omega, \tag{10}$$

it will produce an $R_A C$ time constant in a range from 5.0 fs to 348.5 fs. The capacitance, active area, and $R_A C$ time corresponding to different numbers of electrode are listed in Table 2.

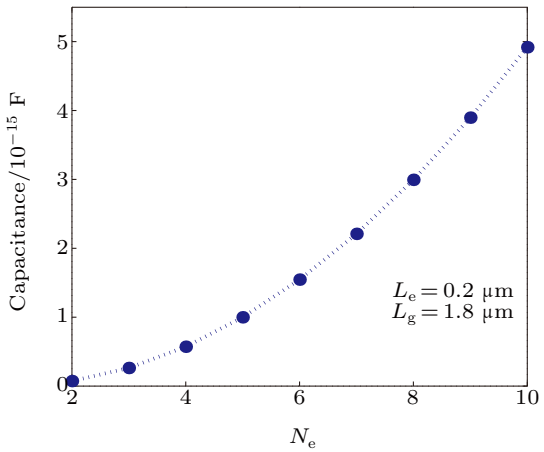


Fig. 4. Plot of electrode capacitance as a function of the electrode number with a fixed gap width and electrode width having optimal values of 1.8 μm and 0.2 μm, respectively.

Table 2. The active area S, capacitance C, and $R_A C$ time verse numbers of electrode N_e with a fixed gap width and electrode width having optimal values of 1.8 μm and 0.2 μm.

	$N_e = 2$	$N_e = 3$	$N_e = 4$	$N_e = 5$	$N_e = 6$	$N_e = 7$	$N_e = 8$	$N_e = 9$	$N_e = 10$
S/μm^2	4.8	17.6	38.4	67.2	104.0	148.8	201.6	262.4	331.2
C/fF	0.07	0.26	0.56	0.98	1.52	2.18	2.95	3.84	4.84
$R_A C$/fs	5.0	18.7	40.3	70.6	109.4	157.0	212.4	276.5	348.5

From Fig. 4 and Table 2, it is clearly shown that the electrode capacitance increases quasi-quadratically with the increase of electrode number. This phenomena can be understood as follows: each of all the gaps between two adjacent electrodes can be modeled by a lumped capacitor connected in parallel as shown in Fig. 5, where C_j represents the increment of finger capacitance when electrode number increases from j to $j + 1$. This equivalent circuit means that new capacitor will be added to this equivalent circuit when the number of electrodes is increased. In light of this model, we find that the values ofthe capacitance sequence are an arithmetical series expressed as

$$\begin{aligned} C_j &= [C_2 + (j-1) \times 0.12]\ [\text{fF}], \\ C_{\text{sum}} &= C_2 + \cdots + C_j + \cdots + C_{N_e - 1} \\ &= \Big[(N_e - 1) \times 0.07 \\ &\quad + \frac{N_e(N_e - 1)}{2} \times 0.12\Big]\ [\text{fF}]. \end{aligned} \tag{11}$$

The first term is 0.07 fF and the common difference is 0.12 fF. According to this model, the capacitance increment and sum capacitance of photomixer can be easily obtained when an electrode is added to the active area. Based on the above analysis, it seems to point out that one should design a photomixer with

fewer electrodes in order to move the 3-dB roll-off point to higher frequency.

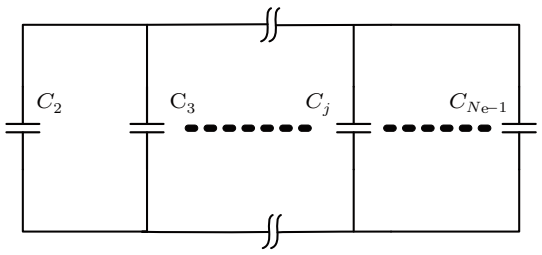


Fig. 5. Lumped capacitance equivalent circuit for the photomixer interdigitated electrode, where C_j ($j > 1$) represents the increment of sum capacitance when the number of electrode increases from j to $j + 1$, C_2 represents the capacitance of photomixer with two electrodes.

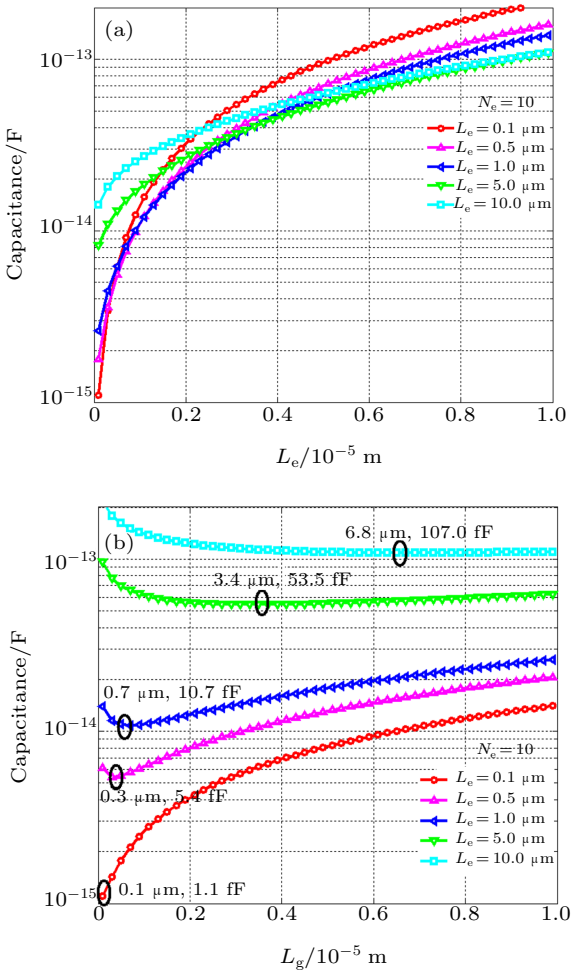


Fig. 6. (colour online) Dependences of finger capacitance and finger parameter with 10 metal fingers. (a) Curves of calculated finger capacitance versus electrode width in different PC gaps of 0.1, 0.5, 1.0, 5.0, and 10.0 μm, and (b) curves of calculated finger capacitance versus PC gap width in different electrode widths of 0.1, 0.5, 1.0, 5.0, and 10.0 μm.

For the practical work, the photomixer seldom has optimum values of 0.2 μm and 1.8 μm as discussed above because the design principle of photomixer may also be based on other standards, such as easy fabrication and thermal burnout. Therefore, it is important to calculate interdigitated finger capacitance as a function of L_e and L_g with a fixed number of electrodes. Figure 6(a) shows plots of the finger capacitance as the function of electrode width at gap widths of 0.1, 0.5, 1.0, 5.0, and 10.0 μm for fixed N_e ($N_e = 10$). At low values of L_e, the finger capacitance increases with the value of L_g increasing from 0.1 μm to 10.0 μm. At high values of L_e, this trend reverses. This extraordinary phenomenon means that it is proper to design interdigitated finger with narrow gap width to attain low finger capacitance in low values of electrode width. In fact, the electrode must be wide enough to being fabricated in lithographic processes and sufficiently robust for withstanding high photocurrents, so high values of gap width should be chosen. In this case, high values of electrode width should be chosen to obtain a relatively low finger capacitance. For the different values of L_e, the finger capacitance first decreases and then increases slightly as L_g increases, which leads to the smallest value of finger capacitance. The smallest capacitances and its corresponding gap width are listed in Fig. 6(b). This means that we can choose an optimal value of gap width L_g to obtain the smallest finger capacitance when electrode width L_e has been defined in advance.

The advantage of using interdigatated fingers in a THz photomixer is that both the length of the metal–semiconductor interface at the electrodes and the conductance can be effectively increased, and hence the impedance match with the PC antenna is improved. The disadvantage is that both capacitance and device heating increase, and hence laser beam drift is induced, which will certainly reduce the output power of CW-THz radiation. In order to overcome these unexpected effects, steps should be taken to solve the incompatibility. First, the active area should be reduced to match the diffraction limitation of the laser beam in order to reduce electrode capacitance, but this should be a compromise in terms of the maximum current limit for device damage. Second, the active area must be large enough for being fabricated by using lithographic processes and sufficiently robust for withstanding high photocurrents, but this is at the expense of the increased capacitance and the drift of the laser beam. Therefore, it is suggested to choose an active area matched to the laser beam diameter and guarantee the device to work properly without thermal damage, and then make a compromise by choosing the proper dimensions of the interdigitated fingers and gaps in the active area in order to reduce finger capac-

itance. Here, we focus on how to design metal electrodes in a constant active area to attain a relatively low finger capacitance. In our calculation, the finger capacitance with an 8 μm × 8 μm active area that was commonly used in previous studies[14,15] is investigated. The active photomixer area can be calculated from $S = [N_e L_e + (N_e - 1)L_g]^2$, for $S = 64$ μm^2, we obtain

$$L_g = (8 - L_e N_e)/(N_e - 1)\,[\mu\text{m}]. \tag{12}$$

Because L_g must be positive, the electrode width L_e should be positive and not more than $8/N_e$. The calculated results are shown in Fig. 7. At low values of L_e, the finger capacitance increases first slowly, then rapidly as L_e reaches relatively high values. Based on this phenomenon, it is better to fabricate metal electrodes with a low value of L_e under the precondition of easy fabrication in order to attain a relatively low finger capacitance in a defined active area. Moreover, it means that we can obtain the same capacitance by using large N_e with small L_e as that by using small N_e with big L_e. For example, if the photomixer is coupled to a 72-Ω spiral PC antenna, 2.75-fF finger capacitance means that the 3-dB roll-off frequency of the power output spectrum is 5 THz. Such device performance can be obtained as shown by the dashed line in Fig. 7, the values of N_e, L_e, and L_g are listed in Table 3. This property will facilitate photomixer design.

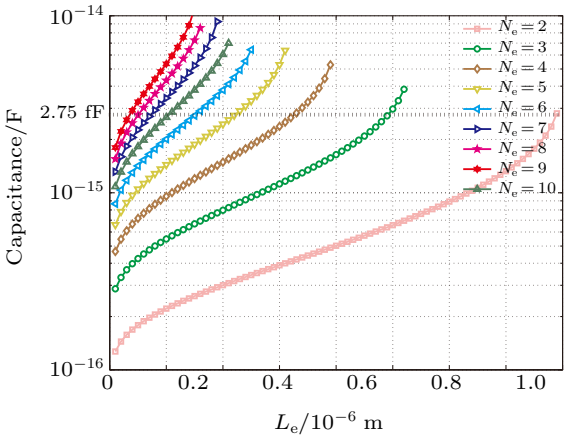


Fig. 7. Curves of finger capacitance of 8 μm × 8 μm active area versus L_e in different values of N_e, with the dashed line representing 2.75 fF finger capacitance.

Table 3. Different values of N_e, L_e, and L_g to form 2.75-fF finger capacitance in 8 μm × 8 μm photomixer.

	$N_e = 2$	$N_e = 3$	$N_e = 4$	$N_e = 5$	$N_e = 6$	$N_e = 7$	$N_e = 8$	$N_e = 9$	$N_e = 10$
L_e/μm	3.94	2.46	1.63	1.10	0.76	0.52	0.36	0.25	0.18
L_g/μm	0.12	0.36	0.49	0.63	0.69	0.73	0.73	0.72	0.69
C/fF	2.75	2.75	2.75	2.75	2.75	2.75	2.75	2.75	2.75

In previous work, by using the method of conformal mappings,[16,17] the values of finger capacitance are analytically calculated by the following equation

$$C \approx \frac{\pi(1+\varepsilon_r)\varepsilon_0 S}{2(L_e + L_g)\log[2(1+\sqrt{\kappa})/(1-\sqrt{\kappa})]},\ (L_e < L_g),$$
$$\kappa = \left\{1 - \tan^4\left(\pi L_e/4\,(L_e + L_g)\right)\right\}^{1/2}. \tag{13}$$

For a photomixer composed of a finger pattern with an active area of 400 μm^2 (64 μm^2) and with 11(4) interdigitated fingers with width 0.3 μm, the finger capacitance is calculated from Eq. (13) to be 2.8 fF (0.5 fF). By using the FEM in this paper, numerical calculations predict the total capacitances to be approximately 6.9 fF and 0.8 fF, respectively. These are consistently greater than the values analytically calculated for similar structures by Eq. (13) because the effect of screening is considered in this simulation. These trends are in good agreement with the experimental results given by McIntosh *et al.*[18] and other simualtions using an electromagnetic simulator.[19] However, the absolute finger capacitances are somewhat different between simulation and experiment. The reason for the difference may be attributed to the thickness of the metal electrode and the imperfect Ohmic contact between metal and LTG-GaAs. In addition, the constraint condition imposed on Eq. (13) is avoided in this simulation. Thus, the results we obtained have a large application scope. According to this, we can fully understand the dependence between device configuration and finger capacitance and provide a guideline to optimize the experimental work.

4. Conclusion

In this paper, we use the FEM to calculate the interdigitated finger capacitances of a THz photomixer with different configurations. Finger capacitance increases almost quadratically with the increase of electrode number, with gap width and electrode width fixed, and this phenomenon can be simply understood by the capacitor originating from interdigitated fingers connected in parallel. For a small electrode width, the finger capacitance increases as the gap width in-

creases, and this trend reverses for a large electrode width. For a constant electrode width, the finger capacitance first decreases and then increases slightly as gap width increases, which leads to the smallest value of finger capacitance and an optimum gap width for designing photomixers. For the most commonly used 8 μm × 8 μm active area, finger capacitance increases slowly at low values of electrode width and then increases rapidly at high values of electrode width. The values of finger capacitance numerically calculated by the FEM are greater than the values calculated from the traditional method of conformal mappings, and are consistent with experimental results. All the calculated finger capacitances at different photomixer configurations can firmly facilitate the design of photomixer to attain a relatively low capacitance under the precondition of easy fabrication, device thermal burnout avoidance, and ease of laser alignment.

References

[1] Brown E R, Smith F W and McIntosh K A 1993 *J. Appl. Phys.* **73** 1480

[2] Verghese S, McIntosh K A and Brown E R 1997 *IEEE Trans. Microw. Theory Tech.* **45** 1301

[3] Gregory I S, Tribe W R, Cole B E, Baker C, Evans M J, Bradley I V, Linfield E H, Davies A G and Missous M 2004 *Electron. Lett.* **40** 143

[4] Stanze D, Deninger A, Roggenbuck A, Schindler S, Schlak M and Sartorius B 2011 *J. Infrared Milli. Terahz. Waves* **32** 225

[5] Marazita S, Hui K, Hesler J, Bishop W and Crowe T 1999 *Proc. 10th Int. Symp. on Space THz Tech.* April 20–22, 1999, Charlottesville, USA, p. 74

[6] Pine A S, Suenram R D, Brown E R and McIntosh K A 1996 *J. Mol. Spectros.* **175** 37

[7] Plusquellic D F, Korter T M, Fraser G T, Lavrich R J, Benck E C, Bucher C R, Walker A R H and Domenech J L 2003 *Int. J. High Speed Electron. Syst.* **13** 385

[8] Knobloch P, Schildknecht C, Ostmann T K, Koch M, Hoffmann S, Hofmann M, Rehberg E, Sperling M, Donhuijsen K, Hein G and Pierz K 2002 *Phys. Med. Biol.* **47** 3875

[9] Preu S, Dohler G H, Malzer S, Wang L J and Gossard A C 2011 *J. Appl. Phys.* **109** 061301

[10] Gregory I S, Baker C, Tribe W R, Evans M J, Beere H E, Linfield E H, Davies A G and Missous M 2003 *Appl. Phys. Lett.* **83** 4199

[11] Gupta S, Frankel M Y, Valdmanis J A, Whitaker J F, Mourou G A, Smith F W and Calawa A R 1991 *Appl. Phys. Lett.* **59** 3276

[12] Zhou W M, Wang C Y, Chen Y H and Wang Z G 2006 *Chin. Phys.* **13** 1742

[13] Ralph S E and Grischkowsky D 1991 *Appl. Phys. Lett.* **59** 1972

[14] Mangeney J, Merigault A, Zerounian N, Crozat P, Blary K and Lampin J F 2007 *Appl. Phys. Lett.* **91** 241102

[15] Hindle F, Cuisset A, Bocquet R and Mouret G 2008 *C. R. Physique* **9** 262

[16] Lim Y C and Moore R A 1968 *IEEE Trans. Electron. Dev.* **ED-15** 173

[17] Brown E R, McIntosh K A, Nichols K B and Dennis C 1995 *Appl. Phys. Lett.* **66** 285

[18] McIntosh K A, Brown E R, Nichols K B, McMahon O B, DiNatale W F and Lyszczarz T M 1995 *Appl. Phys. Lett.* **67** 3844

[19] Gregory I S, Baker C, Tribe W R, Bradley I V, Evans M J, Linfield E H, Davies A G and Missous M 2005 *IEEE J. Quantum Electron.* **5** 717